Sensors and Materials, Vol. 36, No. 9 (2024) 3701–3712
MYU Tokyo

S & M 3760

Enhancement of microRNA Detection Signal Based on Au-nanoparticle-catalyzed Ag Accumulation Observed by Electrochemical and Surface Plasmon Resonance Analyses

Hiroshi Aoki*

Environmental Management Research Institute,
National Institute of Advanced Industrial Science and Technology (AIST),
16-1 Onogawa, Tsukuba, Ibaraki 305-8569, Japan

(Received June 10, 2024; accepted August 5, 2024)

Keywords: electrochemical measurement, surface plasmon resonance imaging, microRNAs, detection, enzymatic amplification

MicroRNAs (miRNAs) are potentially useful biomarkers for the evaluation of cancers and chemical toxicity. However, simply and easily operated detection techniques are increasingly needed to enable their use in the biomedical and environmental fields. In this study, we investigated sequence-specific miRNA detections by surface plasmon resonance (SPR) and electrochemical (EC) imaging measurements on SPR-EC chips possessing a Au electrode array modified with probe DNAs and by employing a miRNA-detection-selective signal amplification method. MiRNAs were sequence-specifically detected by SPR and EC imaging measurements on a single chip. SPR signals were enhanced by a combination process employing the sequence-specific hybridization of miRNAs with the probe DNA, the extension reaction of polyadenine [poly(A)] tails on the 3' end of the miRNAs by poly(A) polymerase, the binding of T_{30}-Au nanoparticles (AuNPs) to the poly(A) tails, and the reduction reaction of Ag^+ catalyzed on the AuNPs, depositing a gray precipitate on the surface. The oxidation reaction of the accumulated Ag precipitation additionally provides EC signal amplification. This process considerably and sequence-specifically amplifies the SPR and EC signals. This setup constitutes a simple and feasible signal amplification method for the on-site detection of miRNA biomarkers.

1. Introduction

MicroRNAs (miRNAs) are short-chained noncoding RNAs (length: 20–25 bases); they control the transcription and decomposition of messenger RNAs (mRNAs), which are coding RNAs that carry genetic information.[1] There have been numerous studies on miRNAs, such as evaluations of stress resulting from exposure to environmental chemicals and their potential applications to miRNA-based diagnoses, including healthcare and cancer detection.[2–4] Many researchers have studied miRNAs, one form of biomarker for cancer, over the past few decades.[5,6] Because miRNAs are present in blood samples and can be collected routinely and

*Corresponding author: e-mail: aoki-h@aist.go.jp
https://doi.org/10.18494/SAM5177

ISSN 0914-4935
https://myukk.org/

relatively noninvasively, they are anticipated to play a role in rapid diagnostic methods in these fields. To apply miRNA detection methods to the biomedical and environmental fields as first screening tools, it is necessary to develop rapid and simple detection methods.[7]

Numerous methods of detecting oligonucleotides have been developed, aiming at rapid and simple screening,[8–13] which is often based on microgravimetric, electrochemical, and optical techniques. Surface plasmon resonance (SPR) imaging (SPRi) is an optical technique that enables the real-time detection of multiple biomolecules without the need to label the target molecules.[10,14–17] Measurements of biomolecules by SPRi are based on the changes in SPR images before and after molecular recognition. Greater numbers of molecules subjected to molecular recognition yield larger changes. Electrochemical sensing also enables the real-time detection of multiple biomolecules without target labeling[18,19] and, moreover, provides advantages in the development of simply designed and compact sensing systems with low energy requirements for detection,[20,21] greatly helping to develop simple and feasible detection systems.

In 2006, Corn and coworkers developed an SPRi-based miRNA detection method that used the hybridization of the target miRNA with the probe DNA on a gold electrode with two-step signal enhancement that combined the poly(A) tail extension reaction and the gold nanoparticle (AuNP) binding reaction.[22] In 2019, as an improved version, we developed a method with three-step signal enhancement that combined the poly(A) tail extension, the horse radish peroxidase (HRP) binding reaction instead of AuNPs, and the tetramethylbenzidine (TMB) oxidative precipitation reaction catalyzed by HRP.[15] These methods successfully detected miRNAs at femtomolar- or attomole-level concentrations for reports in 2006 and 2019, respectively; however, they employ different enzymatic reactions, and the use of the optical system for SPRi requires advanced skills, so they are far from simple.

In this study, therefore, we aimed to establish a miRNA sensing system that combined an SPRi system and an electrochemical sensing system to permit easier and simpler miRNA detection. Specifically, by using the poly(A) tail extension and AuNP binding reactions, and the Ag-reductive precipitation reaction catalyzed on AuNPs for further signal amplification, we attempted to reduce the number of enzymatic reactions required for signal enhancement. At the same time, by converting the final enhanced signal into an electrochemical signal for the Ag redox reaction, we aimed to develop a simple miRNA detection method that does not require advanced skills, in which the system incorporates the advantages of electrochemical sensing to allow simple detection. SPRi and electrochemical sensing were applied at each step in this multiple signal enhancement procedure to investigate the state of each process. The binding reaction of AuNPs to the poly(A) tails was confirmed by SPRi. In addition, since each AuNP is known to act as a nucleation site for the Ag-reductive precipitation reaction,[23–26] we confirmed, using SPRi, that Ag^0 is generated around the AuNP by the reduction of Ag^+ ions on the surface of the AuNP, and that precipitation therefore took place. Moreover, by oxidizing Ag^0 to convert it to Ag^+ ions, we demonstrated electrochemical signals specific to the target miRNA.

We here proposed a novel concept for a miRNA sensing method as a preliminary study by SPRi and electrochemical sensing based on the sequence-specific detection of the target miRNA converted to Ag by reductive precipitation and Ag oxidative desorption reaction. The method is

expected to be used in various fields of miRNA detection as a simple miRNA detection method based on multiple signal enhancement.

2. Materials and Methods

2.1 Reagents

The sequences of the miRNAs used in this study were from the National Center for Biotechnology Information (NCBI). DNAs and RNAs were purchased from Eurofins Genomic Japan (Tokyo, Japan), with the sequences of 5'-ATT TGA CAA ACT GAC A-NH_2-3' (DNA-NH_2, from hsa-miR-223), 5'-AAA AAA AAA AAA AAA AAA AAA AAA AAA AAA AAA-NH_2-3' (A_{30}-NH_2), 5'-biotin-TTT TTT TTT TTT TTT TTT TTT TTT TTT TTT TTT-3' (T_{30}-SH), and 5'-UGU CAG UUU GUC AAA UAC CCC A-3' (Target RNA, from hsa-miR-223). 11-Mercapto-1-undecane amine (MUAM) was from Dojindo (Kumamoto, Japan). Poly-glutamate sodium (p-Glu), 1-ethyl-3-(3-dimethylaminopropyl)-carbodiimide hydrochloride (EDC), N-hydroxysulfosuccinimide (sNHS), 2-aminoethanol (aEtOH), and 10× phosphate-buffered saline (10× PBS) were from Fujifilm Wako Chemicals (Tokyo, Japan). Poly(A) polymerase, proteinase K, sodium dodecyl sulfate (SDS), Au nanoparticles (AuNPs; diameter, 15 nm), Silver Enhancer Kit, and Sigmacoat siliconizing reagent were from Sigma-Aldrich (St. Louis, MO). 1× PBS was prepared from 10× PBS by tenfold dilution. A Silver Enhancer Kit consists of a silver salt (Solution A), an initiator (Solution B), and a fixer ($Na_2S_2O_3$). All aqueous solutions were prepared with deionized and charcoal-treated water (specified resistance >18.2 MΩ cm), obtained using a Milli-Q reagent-grade water system (Merck Millipore; Bedford, MA).

2.2 Preparation of SPRi-EC chips

SPRi-EC chips (3 electrodes; diameter, 12 mm; central angle, 120°) were fabricated in a manner similar to that reported in previous papers.[15] Briefly, a mechanically polished SF-10 glass (Schott Glass; Mainz, Germany) or equivalent (e.g., S-TIH10 from Ohara, Kanagawa, Japan) was cleaned by O_2 plasma emitted from a plasma cleaner. The glass was treated with a Sigmacoat siliconizing reagent for 1 min, rinsed with hexane, ethanol, and water, and baked at 90 ˚C for 1 h. A 10-Å-thick Cr adhesion layer and a 450-Å-thick Au film were deposited on the glass covered with a stencil template of the SPRi chip pattern using a CFS-4EP-LL sputter setup (Shibaura Mechatronics, Kanagawa, Japan). Au surfaces were soaked in a 1 mM MUAM ethanoic solution overnight, 2 mg/mL p-Glu in PBS for 1 h, and a PBS solution containing 75 mM EDC + 15 mM sNHS + 0.25 mM DNA-NH_2 (or A_{30}-NH_2 or aEtOH) overnight, as depicted diagrammatically in Fig. 1(a). The Au surfaces of the chip were modified with DNA-NH_2, A_{30}-NH_2, and aEtOH, as shown in Fig. 1(b). An image of the fabricated SPRi-EC chip is shown in Fig. 1(c). Each electrode has an electric pad for the collection of electrochemical signals.

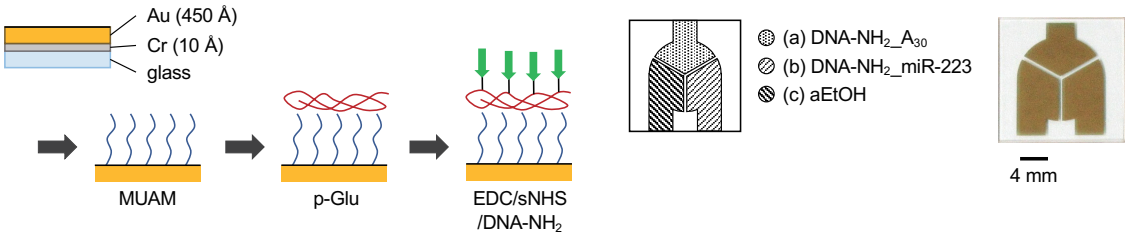

Fig. 1. (Color online) Modification of surface of Au deposited on the glass substrate. (a) The surface was modified with 8-mercaptoundecane amine (MUAM), poly-glutamate sodium (p-Glu), and 1-ethyl-3-(3-dimethylaminopropyl)-carbodiimide hydrochloride (EDC)/*N*-hydroxysulfosuccinimide (sNHS)/DNA-NH_2 or aEtOH). (b) The layouts show DNA-NH_2_A_{30}, DNA-NH_2_miR-223, and aEtOH modified spots for SPRi-EC measurements. (c) Photo of the fabricated SPRi-EC chip.

2.3 miRNA detection

The detection of the target miRNA is briefly outlined in Fig. 2 and is partially similar to the manner described in our previous paper.[15] Thirty microliter aliquots of an RNA solution in PBS were dropped onto the prepared DNA-modified surface of the SPRi-EC chips and left overnight (a). After RNA hybridization, the surface of the chip was covered with a flow cell with a volume of 100 µL, and a flow cell/chip/prism assembly was composed. The solutions were passed through the flow cell at a flow rate of 1 mL/min. Next, the surface was reacted for 30 min with a mixture of 3 U/µL poly(A) polymerase and 1 mM ATP in a reaction buffer as described by Aoki *et al.*,[15] and washed with PBS for 30 min. After the reaction, the surface was washed with 0.1 mg/mL proteinase K in PBS for 30 min, with 0.01% SDS in PBS for 30 min, and then with PBS for 30 min (b). The surface was then reacted with T_{30}-AuNP (optical density of 2 at 518 nm) in PBS for 30 min and then washed with PBS (c). T_{30}-AuNP was prepared as described by Fang *et al.*[22] Finally, the surface was reacted with a 1:1 mixture of a silver salt (Solution A) and an initiator (Solution B) from a Silver Enhancer Kit for 5 min, and washed with PBS for 40 min, followed by washing with 2.5% $Na_2S_2O_3$ for 2 min (d), following the manufacturer's instructions. Ag^+ ions present in the Silver Enhancer Kit are reduced to Ag^0 on AuNPs, which appears as a gray precipitate. The following Ag^0 oxidation desorption reaction to Ag^+ provides electrons to the electrode, leading to further signal enhancement. SPR images were collected before and after each step to obtain difference images by subtraction.

2.4 SPRi measurements

An SPR imager (GWC Technologies; Madison, WI) was used for all the SPRi experiments in the above-mentioned flow cell system based on near-infrared excitation from an incoherent white light source [Figs. 3(a) and 3(b)], as described in our previous paper.[15] Briefly, collimated *p*-polarized light was used to illuminate the flow cell/chip/prism assembly at a fixed incident angle near the SPR angle. The reflected light was directed through a band-pass filter centered at λ = 830 nm and collected using a CCD camera. The data was collected using V++ digital

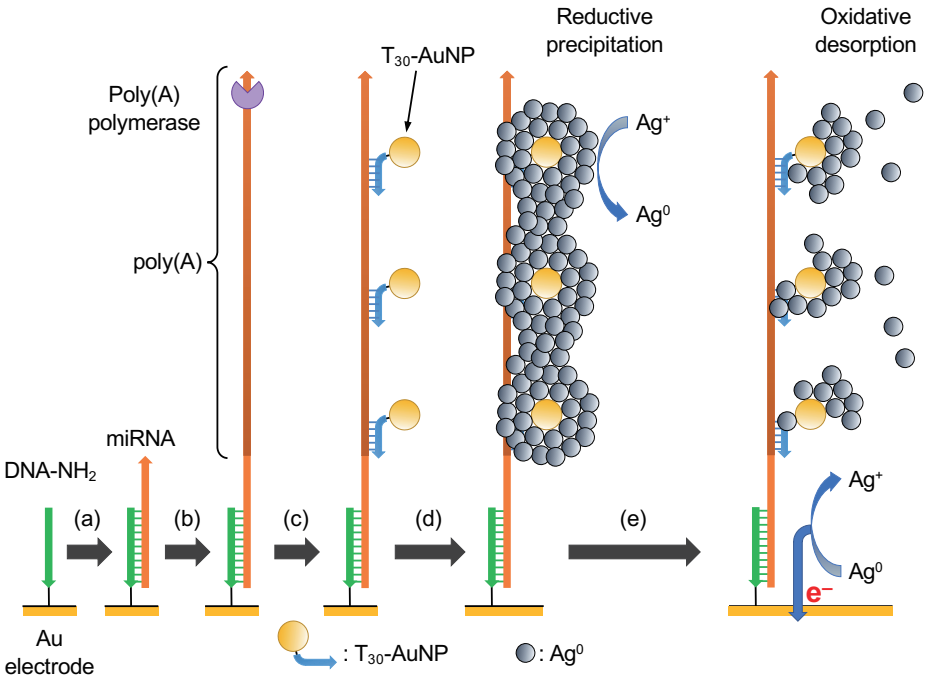

Fig. 2. (Color online) SPR or EC signal amplification process based on enzymatic reactions. (a) The probe DNA-NH_2 tethered to the Au surface is hybridized with the target miRNA. (b) Poly(A) polymerase extends poly(A) tails at the 3' terminal of the target miRNA on the surface. (c) T_{30}-AuNP is bound to the poly(A) tails. (d) Ag^+ is reduced to Ag^0 on AuNPs, which appears as a gray precipitate. (e) The oxidative desorption of Ag^0 to Ag^+ provides electrons to the electrode.

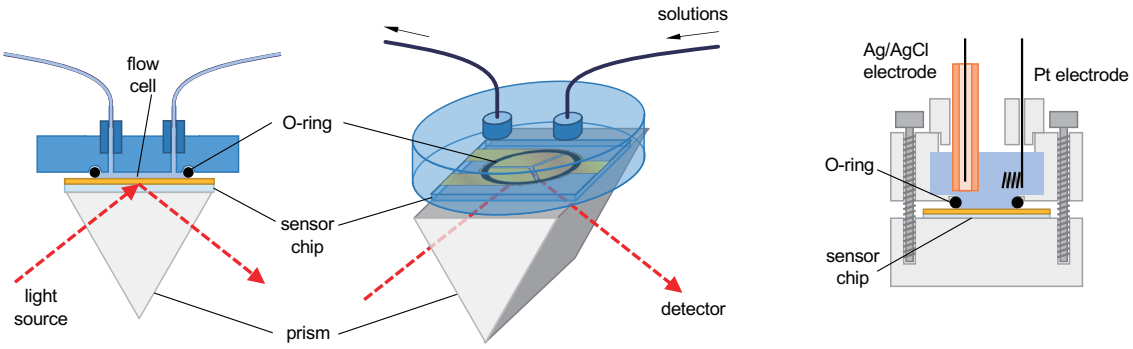

Fig. 3. (Color online) The configuration of the flow cell/chip/prism assembly for SPRi measurements is shown in (a) (side view) and (b) (bird's-eye view). The solutions flow into the flow cell and cover the Au surface. The light from the light source is reflected at the Au surface on the chip through the prism. The configuration for EC measurements is shown in (c) (side view). The measurements were performed on the Au surface terminated by a Cu foil tape.

imaging system software (Digital Optics; Auckland, New Zealand) and further analyzed using ImageJ image analysis software (NIH; Bethesda, MD). For the investigation of the sensor responses, we used the results of SPRi inside the O-ring.

2.5 Electrochemical measurements

Electrochemical measurements were performed at room temperature using a three-electrode configuration consisting of a Ag/AgCl reference electrode (internal solution: 3 M NaCl), a platinum auxiliary electrode, and the prepared electrode as the working electrode, using an ALS 760C electrochemical analyzer (Bioanalytical Systems; Tokyo, Japan) [Fig. 3(c)]. The prepared SPRi-EC chip was connected to the analyzer with a commercially available conductive copper foil tape (width, 5 mm). Cyclic voltammograms (CVs) were recorded with the potential scanned from 0 to +0.5 V and again back to 0 V or scanned from 0 to +0.5 V, then to –0.3, and back to 0 V at a scan rate of 0.1 V s^{-1} in PBS or in PBS containing 1 mM $K_4[Fe(CN)_6]$ as an electroactive marker. For the investigation of the sensor responses, we used the results of the electrochemical measurements inside the O-ring.

3. Results and Discussion

3.1 AuNP-based miRNA-detection-selective signal amplification

In a previous report, we demonstrated miRNA detection by SPRi measurements based on a miRNA-detection-selective SPR signal amplification method. The amplification method consisted of the extension reaction of poly(A) tails by poly(A) polymerase, the binding of a ternary complex of T_{30}-biotin/horseradish peroxidase (HRP)-biotin/streptavidin to the poly(A) tails, and the oxidation reaction of tetramethylbenzidine (TMB) on the HRP by providing a blue precipitate on the surface. In this study, instead of the ternary complex, we tried to demonstrate the amplification of both the SPR and EC signals for miRNA detection by using T_{30}-AuNP and the reduction of Ag^+ on the AuNP by providing a gray precipitate on the surface. More than in the previous study, we focused on processes (c) and (d) in Fig. 2 for the amplification of the SPR and EC signals.

In Fig. 4(A), we show the SPR image obtained after the hybridization of the target RNA to the surface-immobilized probe DNA and the following poly(A) extension reaction [after process (b) in Fig. 2]. This figure does not explicitly illustrate the miRNA-selective SPR signal amplification among the three electrodes. A comparison of the grayscale values, however, reveals a significant increase in SPR signal for electrode (b). The average grayscale value for electrode (b) in Fig. 4(A) was 96.8 ± 5.63, whereas those for electrodes (a) and (c) were 94.8 ± 3.34 and 83.5 ± 4.87, respectively. Although the change in the SPR image was not marked, the results are consistent with those reported in our previous paper, in which miRNA-selective signal amplification was confirmed. Next, Fig. 4(B) shows the SPR image obtained after the binding of T_{30}-AuNP [after process (c) in Fig. 2]. Figure 4(C) shows an image of the subtraction between the images obtained before and after the binding of T_{30}-AuNP. These figures clearly illustrate the SPR signal amplification on electrode (c). It thus appears that the electrode had been modified with aEtOH and that the nonspecific adhesion of T_{30}-AuNP occurred. Here, T_{30}-AuNP has a T_{30} unit and was expected to show sequence-selective binding with not only the poly(A) tail but also with A_{30}, although binding to the poly(A) tails is not recognizable at the electrodes immobilized with

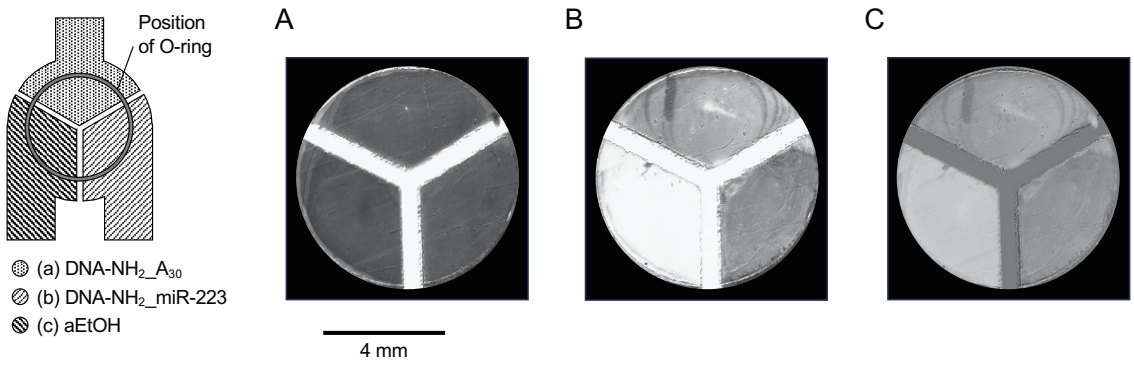

Fig. 4. SPR images obtained after the treatments of (b) and (c) depicted in Fig. 2 for (A) and (B), respectively. (C) was obtained from subtraction between (B) and (A). In each image, the areas for the sensors for DNA-NH_2_A_{30}, DNA-NH_2_miR-223, and aEtOH are indicated as a, b, and c, respectively.

them in the SPR image in Fig. 4(C). This phenomenon is considered to be due to the nonspecific adsorption of T_{30}-AuNP to electrode (c), but there may be other explanations. Electrochemical measurements were carried out to acquire more detailed information.

Figure 5 shows electrochemical measurements for the three electrodes after process (c) in Fig. 2. Figure 5(a) shows cyclic voltammograms (CVs) measured in PBS for electrodes (a), (b), and (c) depicted in Fig. 4. Lower charging currents were observed for electrodes (a) and (b), whereas for electrode (c), in contrast, a higher charging current was observed. These results indicate that the electrolyte ions are more inhibited from accessing the surfaces of electrodes (a) and (b). This inhibition appears to be due to the steric hindrance caused by the T_{30}-AuNP bound to these electrodes, although this binding is vague in the SPR results, revealing the sequence-specific binding of T_{30}-AuNP to A_{30} and poly(A) tails. Figure 5(b) shows CVs for these electrodes measured in PBS containing 1 mM $[Fe(CN)_6]^{4-}$. Electrode (c) shows a quasi-reversible CV with high oxidation and reduction peaks for the redox reaction of $[Fe(CN)_6]^{4-}$, whereas electrodes (a) and (b) show a totally irreversible CV with no peaks for $[Fe(CN)_6]^{4-}$. These results indicate electrostatic repulsion between $[Fe(CN)_6]^{4-}$ and the negative charges on the DNAs (A_{30}, poly(A) tails, and T_{30}) and demonstrate that the above-mentioned steric hindrance inhibits the redox reaction of $[Fe(CN)_6]^{4-}$ on the electrode surface.

These results allow us to conclude from the electrochemical measurements that T_{30}-AuNP sequence-selectively binds to A_{30} or poly(A) tails on electrodes (a) and (b), respectively. We therefore moved on to the next amplification step.

3.2 Ag-oxidation-based miRNA-detection-selective signal amplification

Signal amplification based on T_{30}-AuNP showed no definite signal heightening in the SPR measurements; however, the electrochemical measurements showed sequence-selective responses. AuNPs can thus act as a catalyst for Ag-reductive precipitation from silver solution.[24–26] For instance, Ag-reductive precipitation is generally used in the field of gel electrophoresis to enhance optical signals for the easy detection of separated analytes. In this

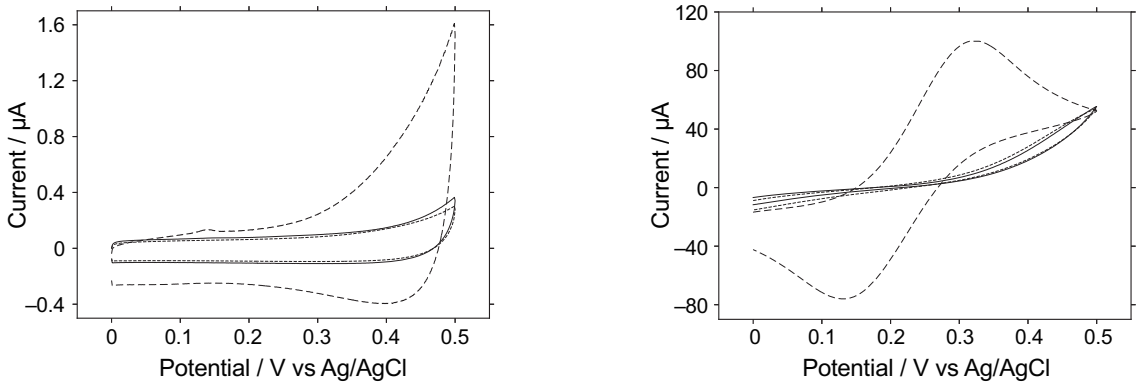

Fig. 5. CVs measured in (a) PBS or (b) PBS with 1 mM $[Fe(CN)6]^{4-}$ after treatment (c) depicted in Fig. 2 for the sensors for DNA-NH_2_A_{30} (solid, Fig. 4(a)), DNA-NH_2_miR-223 (dotted, Fig. 4(b)), and aEtOH (dashed, Fig. 4(c)).

study, we utilized the Ag-reductive precipitation method to enhance the signals from AuNP sequence-specific binding to A_{30} or poly(A) tails. Figure 6 shows the SPR images obtained after process (d) in Fig. 2 for Ag-reductive precipitation at the AuNP on the electrode surface. Figure 6(A) indicates that the Ag precipitation provided via the reductive reaction of Ag^+ enhanced the SPR signals. Figure 6(B), derived from subtraction between Figs. 6(A) and 4(B), shows that Ag precipitation occurred on the surfaces of electrodes (a) and (b), significantly enhancing the SPR signals. The average grayscale values for electrodes (a) and (b) were 162.7 ± 4.8 and 165.6 ± 3.5, respectively, in contrast to that for electrode (c), which was 127.7 ± 0.5. The fact that Ag-reductive precipitation was seen to a lesser extent in (c) indicates that the AuNP on (a) and (b) caused the precipitation and, in addition, shows T_{30}-AuNP to be sequence-specifically bound to A_{30} and poly(A) tails.

Figure 7 shows CV results for the electrochemical process (e) in Fig. 2 for the oxidative desorption of Ag precipitated onto the electrodes. Electrode (a) demonstrated two strong and sharp peaks at 0 and +0.12 V. The potential for the Ag redox reaction is around 0 vs Ag/AgCl,[27–29] so these results therefore show the redox reaction leading to Ag precipitation resulting from the reductive reaction of Ag^+ at AuNP on the electrode surface. On the other hand, electrode (b) illustrated two more significant peaks at –0.04 and +0.2 V that can be attributed to the Ag redox reaction. Because the area of the peaks for the Ag redox reaction is considered to be proportional to the numbers of electrons involved in the reaction ($Ag^0 \rightarrow Ag^+ + e^-$),[30] the numbers of electrons for electrodes (a) and (b) were calculated to be 47.1 and 112 µC, respectively. From these results, electrode (b) has 2.4-fold greater Ag precipitation than electrode (a). On the basis of the previous reports,[15,22] we conclude that the poly(A) tail reaches around 250 adenosine residues for electrodes (a) and (b) under the conditions applied during this study. The number of T_{30}-AuNP complexes bound to the poly(A) tails in electrode (b) is likely to be eightfold that of A_{30} on electrode (a). Considering the rather large size of the AuNPs, leading to their blocking of binding due to steric hindrance, it is unsurprising that the result does not match the calculations in the electrochemical study. It can be concluded that the resultant signal was significantly enhanced by the reaction causing Ag-reductive precipitation.

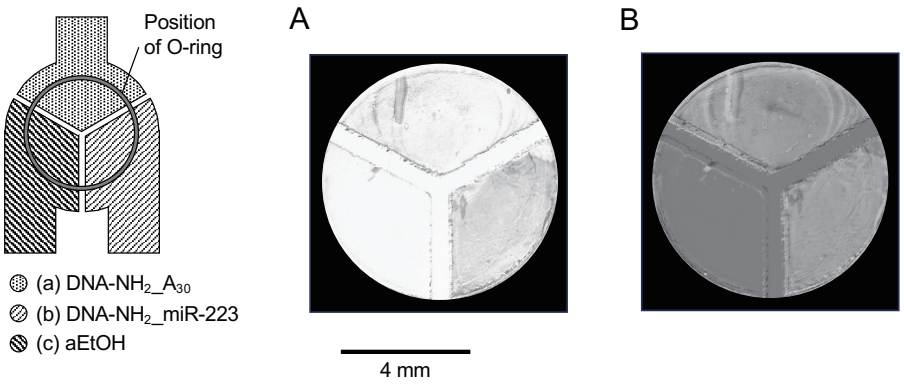

Fig. 6. SPR images obtained after treatment (d) depicted in Fig. 2 for (A). (B) was obtained from subtraction between (A) and Fig. 4(B). In each image, the areas for the sensors for DNA-NH_2_A_{30}, DNA-NH_2_miR-223, and aEtOH were indicated as a, b, and c, respectively.

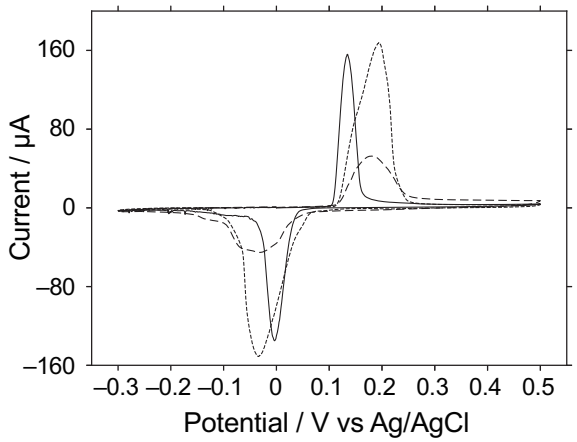

Fig. 7. CVs measured in PBS for treatment (e) depicted in Fig. 2 for the sensors for DNA-NH_2_A_{30} (solid, Fig. 6(a)), DNA-NH_2_miR-223 (dotted, Fig. 6(b)), and aEtOH (dashed, Fig. 6(c)).

On the other hand, small peaks were observed for electrode (c), which were much lower than those for electrodes (a) and (b). This is because only a small number of T_{30}-AuNP complexes were present on the electrode surface and, as a result, little Ag was precipitated. Although this result appears to contradict the SPR image in Fig. 4(B), which showed an identifiable SPR signal for electrode (c), this demonstrates that the selective reaction definitely occurred.

Moreover, the CVs in Fig. 7 show separate peak potentials for the Ag redox reaction of around 0.12–0.2 V. The Ag involved in the redox reaction is a surface-confined species, expected to have a peak potential separation of 0 V. However, the results showed that a large overpotential was applied to the oxidative reaction of Ag. This behavior is similar to previously reported results on the electrochemistry of Ag nanoparticles.[28,29] This means that the reaction needs higher potential, indicating that the reduction of Ag occured such that Ag was clustered on the AuNP surface as a catalyst, leading to the need for higher potential to activate Ag oxidation.

3.3 Limitations and advantages of this technique

The purpose of the technique outlined in this study is to enhance signals for the detection of miRNAs by using a combination of AuNPs and Ag, and to upgrade the technique described in Fang *et al.*'s 2006 study or miRNA detection based on AuNPs.[22] We confirmed the AuNP binding reaction and Ag-reductive precipitation via SPRi and the presence of the precipitated Ag by the oxidative desorption of Ag. We confirmed the concept behind this enhanced technique using the biomarker miRNAs present in the blood of lung cancer patients. More investigations are now possible into the potential detection limit and quantitative reproduction as an analytical method.

Owing to the requirement for Au and Ag, this technique is more costly than our previously reported technique for the signal enhancement of RNA detection that was based on the oxidative precipitation of TMB, an organic molecule.[15] However, the new technique is more practical and convenient for identifying the presence of target miRNAs because it generates results using fewer numbers of enzymes. It may be possible to cut the use of Au and Ag by reducing the sizes of the electrodes and/or reusing precious metals, specifically the AuNPs that dissociated from the extended poly(A) tails and the Ag ions that underwent oxidative desorption.

4. Conclusions

In this study, we demonstrated the SPRi and EC signal enhancement of miRNA detection by using the sequence-specific recognition of target miRNAs by probe DNAs immobilized on the gold electrode surface, the extension of poly(A) tails from miRNA terminals, the binding of T_{30}-AuNP to the poly(A) tails, and the Ag-reductive precipitation on AuNPs. To confirm the signal enhancement achieved by SPRi, although SPRi showed the nonspecific adsorption of AuNPs on the surface, the following Ag-reductive precipitation revealed a sequence-specific signal increase with the miRNA and A_{30} sensors (positive control). Electrochemical studies showed the oxidative desorption of Ag reductively precipitated and the re-reductive precipitation on the miRNA sensor. In this study, we focused on the development of a simple procedure for SPR and EC signal amplification based on the combination of poly(A) tail extension and Ag precipitation on AuNPs. Although further investigations might be needed to identify the detection limits and reproducibility of this method, we successfully demonstrated here the concept of a novel method for enhancing miRNA detection signals.

The miRNA selected in this study was an RNA lung cancer biomarker.[15] However, our developed method covers various RNAs, not only miRNAs. In RNA expression analysis, for example, which is performed in the fields of biological evaluation of chemicals[31–33] and gene analysis of enzymes produced by microorganisms,[34,35] the sequences of expressed RNAs are sometimes known in advance prior to the analysis, allowing the analysis to focus on specific RNAs with known sequences. Here, it is possible to prepare probe DNAs possessing sequences complementary to the target RNAs for this method and to employ the prepared sensor array for the analysis of these RNAs. Next-generation sequencers (NGSs) are commonly used for comprehensive RNA analysis, but, if the specific sequences are known beforehand as targets,

NGSs will both overperform the analysis and require laborious processes that depend on trained personnel. Our developed technique, on the other hand, is based on SPR imaging and EC, and readily yields results due to its focus on detecting specific RNAs. We anticipate that this developed technique can be further improved and applied to a broader range of fields related to RNA analysis.

Acknowledgments

This work was partially supported by JSPS KAKENHI Grant Number JP19K05536 (awarded to H.A.).

References

1 H. Siomi and M. C. Siomi: Mol. Cell **38** (2010) 323. https://doi.org/10.1016/j.molcel.2010.03.013
2 S. Kreth, M. Hübner, and L. C. Hinske: Anesth. Analg. **126** (2018) 670. https://doi.org/10.1213/Ane.0000000000002444
3 M. Olejniczak, A. Kotowska-Zimmer, and W. Krzyzosiak: Cell. Mol. Life Sci. **75** (2018) 177. https://doi.org/10.1007/s00018-017-2591-0
4 W. Y. Hong and C. C. William: Arch. Toxicol. **89** (2015) 319. https://doi.org/10.1007/s00204-014-1440-2
5 S. L. Hofbauer, M. de Martino, I. Lucca, A. Haitel, M. Susani, S. F. Shariat, and T. Klatte: Urol. Oncol. **36** (2018) 531.e1. https://doi.org/10.1016/j.urolonc.2018.09.006
6 D. Bonci, V. Coppola, M. Patrizii, A. Addario, A. Cannistraci, F. Francescangeli, R. Pecci, G. Muto, D. Collura, R. Bedini, A. Zeuner, M. Valtieri, S. Sentinelli, M. S. Benassi, M. Gallucci, P. Carlini, S. Piccolo, and R. De Maria: Oncogene **35** (2016) 1180. https://doi.org/10.1038/onc.2015.176
7 R. Fiammengo: Biomark. Med. **11** (2017) 69. https://doi.org/10.2217/bmm-2016-0195
8 J. Wu, H. Liu, W. Chen, B. Ma, and H. Ju: Nat. Rev. Bioeng. **1** (2023) 346. https://doi.org/10.1038/s44222-023-00032-w
9 J. Qin, W. Wang, L. Gao, and S. Q. Yao: Chem. Sci. **13** (2022) 2857. https://doi.org/10.1039/d1sc06269g
10 C. Coutinho and A. Somoza: Anal. Bioanal. Chem. **411** (2019) 1807. https://doi.org/10.1007/s00216-018-1450-7
11 R. M. Graybill and R. C. Bailey: Anal. Chem. **88** (2016) 431. https://doi.org/10.1021/acs.analchem.5b04679
12 J. Shen, Y. Li, H. Gu, F. Xia, and X. Zuo: Chem. Rev. **114** (2014) 7631. https://doi.org/10.1021/cr300248x
13 D. Chen, N. Chen, F. Liu, Y. Wang, H. Liang, Y. Yang, and Q. Yuan: Anal. Chem. **95** (2023) 1847. https://doi.org/10.1021/acs.analchem.2c03156
14 E. Mauriz: Biosensors **10** (2020). doi: https://doi.org/10.3390/bios10060063
15 H. Aoki, R. M. Corn, and B. Matthews: Biosens. Bioelectron. **142** (2019) 111565. https://doi.org/10.1016/j.bios.2019.111565
16 R. Liu, Q. Wang, Q. Li, X. Yang, K. Wang, and W. Nie: Biosens. Bioelectron. **87** (2017) 433. https://doi.org/10.1016/j.bios.2016.08.090
17 G. Spoto and M. Minunni: J. Phys. Chem. Lett. **3** (2012) 2682. https://doi.org/10.1021/jz301053n
18 H. Aoki, M. Torimura, and T. Nakazato: Biosens. Bioelectron. **136** (2019) 76. https://doi.org/10.1016/j.bios.2019.04.047
19 H. Aoki: Chem. Asian J. **10** (2015) 2560. https://doi.org/10.1002/asia.201500449
20 E. Paleček and M. Bartošík: Chem. Rev. **112** (2012) 3427. https://doi.org/10.1021/cr200303p
21 A. J. Bard and L. R. Faulkner: In Electrochemical Methods: Fundamentals and Applications (John Wiley & Sons, New York, 2001).
22 S. Fang, H. J. Lee, A. W. Wark, and R. M. Corn: J. Am. Chem. Soc. **128** (2006) 14044. https://doi.org/10.1021/ja065223p
23 P. Jiang, Y. Wang, L. Zhao, C. Ji, D. Chen, and L. Nie: Nanomaterials **8** (2018) 977. https://doi.org/10.3390/nano8120977
24 M. Yang and C. Wang: Anal. Biochem. **385** (2008) 128. https://doi.org/10.1016/j.ab.2008.10.019
25 S.-J. Park, T. A. Taton, and C. A. Mirkin: Science **295** (2002) 1503. https://doi.org/10.1126/science.1067003
26 T. A. Taton, C. A. Mirkin, and R. L. Letsinger: Science **289** (2000) 1757. https://doi.org/10.1126/science.289.5485.1757

27 Y.-J. Choi and T.-J. M. Luo: Int. J. Electrochem. **2011** (2011) 1. https://doi.org/10.4061/2011/404937
28 G. Wang, W. Wang, J. Wu, H. Liu, S. Jiao, and B. Fang: Microchim. Acta **164** (2009) 149. https://doi.org/10.1007/s00604-008-0050-1
29 Z.-J. Jiang, C.-Y. Liu, and Y.-J. Li: Chem. Lett. **33** (2004) 498. https://doi.org/10.1246/cl.2004.498
30 A. J. Bard and L. R. Faulkner: In Electrochemical Methods: Fundamentals and Applications (John Wiley & Sons, New York, 2001) p. 590.
31 H. Aoki, H. Tani, K. Nakamura, H. Sato, M. Torimura, and T. Nakazato: Toxicol. Appl. Pharmacol. **392** (2020) 114929. https://doi.org/10.1016/j.taap.2020.114929
32 S. Campion, J. Aubrecht, K. Boekelheide, D. W. Brewster, V. S. Vaidya, L. Anderson, D. Burt, E. Dere, K. Hwang, S. Pacheco, J. Saikumar, S. Schomaker, M. Sigman, and F. Goodsaid: Expert Opin. Drug Metab. Toxicol. **9** (2017) 1391. https://doi.org/10.1517/17425255.2013.827170
33 J. Borlak: In Handbook of Toxicogenomics (Wiley-VCH, New York, 2005).
34 Y. Sato, T. Hamai, T. Hori, T. Aoyagi, T. Inaba, K. Hayashi, M. Kobayashi, T. Sakata, and H. Habe: J. Hazard. Mater. **423** (2022) 127089. https://doi.org/10.1016/j.jhazmat.2021.127089
35 S. Yooseph, K. H. Nealson, D. B. Rusch, J. P. McCrow, C. L. Dupont, M. Kim, J. Johnson, R. Montgomery, S. Ferriera, K. Beeson, S. J. Williamson, A. Tovchigrechko, A. E. Allen, L. A. Zeigler, G. Sutton, E. Eisenstadt, Y. H. Rogers, R. Friedman, M. Frazier, and J. C. Venter: Nature **468** (2010) 60. https://doi.org/10.1038/nature09530